Effective viscosity in filament networks with cross-link slip

William McFadden, Edwin Munro

University of Chicago, Institute for Biophysical Dynamics, Chicago, IL 60615

(Dated: this day)

Abstract

Here we combine theoretical and computational approaches to explore mechanisms that govern long timescale deformation in semi-flexible filament networks with transient cross-links. We introduce a coarse-grained representation of cross-link dynamics in which cross-linked filaments slip past one another with an effective friction representing the time-averaged contributions of transient elastic cross-links. For small strains, we obtain a theoretical prediction for the long timescale effective viscosity of the network that depends on network architecture and effective friction coefficient between filaments, and we confirm this prediction using numerical simulations. We show computationally that network response deviates significantly from purely viscous creep when networks undergo large strains that drive them into anisotropic configurations. Interestingly, under certain conditions, we find a phase of long-lived sub-linear creep, suggesting that our simple model may account for the long-lived transitional phase between purely elastic and purely viscous rheology as measured in actin biopolymer experiments. Finally, we extend our approach to include nonlinear extension of filaments and show that, in certain regimes, this property can endow networks with long-lived strain memory.

CONTENTS

I. INTRODUCTION

Cross-linked networks of semi-flexible polymers are a class of materials with poorly understood but highly interesting properties. Early studies of semi-flexible polymer networks reconstituted *in vitro* revealed novel, nonlinear rheology, spurring interest from materials scientists[6]. Cross-linked networks of cytoskeletal polymers have been a subject of great interest to biologists because of their importance as structural components of cells[13, 36].

On shorter timescales, the response of cross-linked polymer networks to applied stress can be well-described theoretically in terms of purely elastic mechanical resistance. On longer timescales, the network's elastic resistance begins to give way to a viscous relaxation of stored stress, but the mechanisms that govern this viscous relaxation remain poorly understood. It is important to understand the mechanism behind this long timescale relaxation of cross-linked polymer networks both for understanding their novel material properties as well as understanding how this effect may govern physiologically important cellular processes[39].

For *in vitro* reconstitutions, this viscous relaxation is thought to result from transient unbinding and rebinding of intermolecular cross-links[5, 43]. However, there is still no clear understanding of how local relaxations of network connectivity would give rise to a global viscous relaxation. In our work, we wish to expand upon a well-established mechanical picture of cross-linked semi-flexible polymer networks to incorporate slippage of cross-links over longer timescales.

A. Short Timescale Mechanics of Cross-linked Actin Filament Networks

Early *in vitro* studies of cross-linked actin filament networks revealed strikingly different elastic behaviors compared to the already well-understood flexible polymer gels [41]. The complexity of these behaviors drove a surge in both experimental and theoretical studies of semi-flexible networks. For a comprehensive review of this field we recommend [6], but we

will shortly repeat some important milestones here.

1. Theories of Semi-flexible Filament Networks

Diversity and discrepancy in observations led a drive toward systematic *in vitro* experimental explorations of the rheology of cross-linked semi-flexible polymer networks at short timescales. In studies with rigid irreversibly cross-linked networks, it was found that differences in network structure could lead to remarkably different elastic moduli, suggesting distinct phases of mechanical response [16]. These discoveries in turn begat theoretical work on the basic implications of the semi-flexible nature of filaments on network mechanics.

Prior work on the basic physics of individual semi-flexible polymers [9, 31], and comprehensive theories of semi-flexible filament solutions, [33] laid a groundwork for theoretical considerations of cross-linked networks. Beginning with the so-called "mikado model" descriptions[17, 46], it was determined that there should exist a minimum rigidity percolation threshold, and that the connectivity of the network determined whether the mechanical response was dominated by non-affine bending or affine stretching of filaments. Continuing to more explicit theories[40], the mechanics of rigidly cross-linked networks were shown to be well-described in terms of purely elastic stretching of filaments between cross-linked points.

2. Incorporating Effects of Cross-link Compliance

Despite the success of the theory for rigid cross-links, early studies showed that surprising qualitative differences in mechanical response could be traced to differences in the chosen cross-linker[28, 45]. In addition, many studies using more compliant cross-linkers showed that cross-linker compliance could give rise to different nonlinear rheological properties on short timescales[14, 15, 22, 29]. Making matters even more complicated, ongoing research has begun to uncover added complexity from more highly complex issues such as filament bundling[8, 34]and the effects of active cross-linking by molecular motors[24].

While theorists have built a number of largely successful models that help characterize different aspects of the cross-link dominated response[4, 18, 47], the diversity of behaviors of these networks makes a precise yet general theory more difficult.

B. Long Timescale Stress Relaxation from Transient Cross-link Unbinding

At long timescales, the purely elastic behavior of cross-linked networks gives way to fluid-like stress relaxation. Additionally, fluid-like flows have been observed in a number of cellular processes[2, 3, 11, 19, 20, 32]. In *in vitro* studies, long timescale creep behaviors are thought to arise predominantly from the transient nature of filament binding for most biologically relevant cross-linkers[26, 27, 30, 48]. While the importance of cross-link dynamics in determining the mechanical response of semi-flexible polymer networks has been known for at least 20 years[43], there is still a gap in our understanding of how microscopic cross-link unbinding relates to viscous flows.

1. Models of Stress Relaxation with Transient Cross-links

The dependence of network rheology on cross-link unbinding is an active subject of theoretical research[34].

Several theoretical methods have addressed cross-link binding and unbinding directly [5, 34] in analytical approaches that allowed well-constrained fits for specific cross-linkers. These theories have therefore focused conceptually at the level of the cross-linked filament and were extended analytically to macroscopic networks. In another approach, modelers have taken cross-links as extended springlike structures [23] that are able to bind and unbind in simulated filament networks. Finally, other more ambitious simulations have even sought to interrogate the effects of cross-link unbinding in combination with the more complex mechanics of filament bundles[25, 27].

Ultimately, the complexity of the many theoretical approaches that have been applied to this problem have made it difficult to distinguish what, if any, core physical mechanisms may be sufficient to explain the observed forms of stress relaxation. We believe that serious qualitative understanding can be generated by focusing on some of the common elements exhibited in the aforementioned literature.

2. Novelty of Cross-link Slip Approach

Here, we introduce a coarse-grained representation of filament cross-linking in which cross-linked filaments which are able to slide past each other as molecular bonds form and

rupture, akin to coarse-grained models of molecular friction[12, 38, 42]. This drag-like coupling has been shown to be an adequate approximation in the case of ionic cross-linking of actin[7, 44], and can be found in the theoretical basis of force-velocity curves for myosin bound filaments[1]. We propose that it will form a suitable bulk approximation in the presence of super molecular cross-links as well.

Importantly, this simplification allows us to extend our single polymer models to dynamical systems of larger network models for direct comparison between theory and modeling results. This level of coarse graining will therefore make it easier to understand classes of behavior for varying compositions of cross-linked filament networks. In addition, it allows us to compute a new class of numerical simulations efficiently, which gives us concrete predictions for behaviors in widely different networks with measurable dependencies on molecular details.

II. EXPLANATION OF MODEL

A. Composite Cross-link & Filament Representation

We consider individual filaments as chains of springs with relaxed length l_s. The orientations of neighboring springs are linearly coupled. Filaments can therefore be represented as a sequence of nodes with positions $\mathbf{x_i}$ and nearest neighbor interactions of the form

$$|F_{i,i+1}|_{\parallel} = -\mu \cdot \frac{|\mathbf{x_{i+1}} - \mathbf{x_i}| - l_s}{l_s} \tag{1}$$

$$|F_{i,i+2}|_{\perp} = -\frac{\kappa}{l_s^2} \cdot acos\left(\frac{\mathbf{x_{i+2}} - \mathbf{x_{i+1}}}{|\mathbf{x_{i+2}} - \mathbf{x_{i+1}}|} \cdot \frac{\mathbf{x_{i+1}} - \mathbf{x_i}}{|\mathbf{x_{i+1}} - \mathbf{x_i}|}\right) \tag{2}$$

This is essentially a discretized equivalent to a model of filaments with separable extensional and bending moduli as in [17] with a potential defined by

$$\mathcal{H} = \frac{1}{2}\kappa \int ds(\nabla^2 \mathbf{u})^2 + \frac{1}{2}\mu \int ds \left(\frac{dl(s)}{ds}\right)^2 \tag{3}$$

where, μ represents an extensional modulus of a filament, and κ represents a bending modulus.

Here, we take the extensional and bending moduli as composite quantities related to both filament and cross-linker compliance in a manner similar to a recently proposed effective

medium theory[4]. We provide a molecular level derivation of this composite compliance in Appendix C. Here, we highlight the main features.

In the limit of highly rigid cross-links and flexible filaments, our model reduces to the pure semi-flexible filament models of [17, 46]. In the opposite regime of nearly rigid filaments and highly flexible cross links, our method is still largely similar to the model of [4] in small strain regimes before any nonlinear cross link stiffening. However, in departure from those models, the magnitude of the force on interior cross-links in our model is still the same as those on the exterior. This is a simplification of the varying levels of strain that would actually be present in these cross-linkers as addressed in [4], but we choose to ignore the slight variation in favor of an approximated, global mean approach.

B. 2D Network Formation

We choose to focus our attention on 2D networks both for their tractability as well as their relevance in the quasi-2D cytoskeletal cortex of many eukaryotic cells[32]. In addition, recent developments in 2D *in vitro* systems[35, 37], make 2D models all the more interesting as a renewed focus of study.

We follow a mikado model approach by initializing a minimal network of connected unstressed linear filaments in a rectangular 2D domain. We generate 2D networks of these semi-flexible filaments by laying down straight lines of length, L, with random position and orientation. We then assume that some fixed fraction of overlapping filaments become cross-linked (defined in II C) at their point of overlap.

Although real cytoskeletal networks may form with non-negligible anisotropy, we focus on isotropically initialized networks for simplicity. We define the density using the average distance between cross-links along a filament, l_c. A simple geometrical argument can then be used to derive the number of filaments filling a domain as a function of L and l_c[17]. Here, we use the approximation that the number of filaments needed to tile a rectangular domain of size $W \times H$ is $2WH/Ll_c$, and that the length density is therefore $1/l_c$.

In the absence of cross-link slip, we expect the network to form a connected solid with a well defined elastic modulus[17, 46]. These networks are only well-connected when the ratio of filament length to intercross-link spacing, L/l_c, is greater than ~ 6. Near this percolation threshold, there are only locally connected domains, and discussions of global network

properties becomes less reasonable. Additionally, as the filament density is increased beyond this point, there is another transition between non-affine bending and affine stretching of filaments, which changes the dominating term of the network's elastic modulus.

C. Drag-like Coupling Between Overlapping Filaments

In contrast to previous models, we allow relaxation of the network's stored stress by letting the attachment points slip. We do this by replacing an elastic interaction between pairs of points along filaments with a drag-like coupling between filaments.

$$\mathbf{F_{drag}} = \xi \cdot \int ds \, (\mathbf{v(s)} - \mathbf{v_0(s)}) \, f(s) \tag{4}$$

Where $f(s)$ represents the locational distribution of cross-link points (equal to 1 at locations of cross-links and 0 elsewhere). This model assumes a linear relation between applied force and the velocity difference between attached filaments. Obviously, non-linearities can arise in the presence of force dependent detachment kinetics as well as non-linear force extension of cross-links. We address non-linear effects of stress induced unbinding in Appendix B. Assuming inhomogeneities from non-linear effects are of second order, the motion for the entire network is governed by a dynamical equation of the form

$$\int ds \, (\zeta \mathbf{v_i(s)} + \xi \sum_j (\mathbf{v_i(s)} - \mathbf{v_j(s)}) \, p_{ij}(s)) = \nabla \mathcal{H}_i \tag{5}$$

Here, the first term in the integral is the filament's intrinsic drag through its embedding fluid, ζ, while the second comes from the drag-like coupling between filaments, ξ.

D. System of Equations for Applied Stress

We model our full network as a coupled system of differential equations satisfying 5. Although the general mechanical response of this system may be very complex, we focus our attention on low frequency deformations and the steady-state creep response of the system to an applied stress. To do this we introduce a fixed stress, σ along the midline of our domain. This stress points in the direction, $\hat{\mathbf{u}}$, producing either shear ($\hat{\mathbf{u}} = \hat{\mathbf{x}}$) or extensional ($\hat{\mathbf{u}} = \hat{\mathbf{y}}$) stress.

Finally, we add a 0 velocity constraint at the far edges of our domain of interest. We assume that our network is in the "dry," low Reynold's number limit, where inertial effects are so small that we can equate our total force to 0. Therefore, we have a dynamical system of wormlike chain filaments satisfying

$$\int ds \, (\zeta \mathbf{v_i}(\mathbf{s}) + \xi \sum_j (\mathbf{v_i}(\mathbf{s}) - \mathbf{v_j}(\mathbf{s})) \, p_{ij}(s)) = \nabla \mathcal{H}_i + \sigma \hat{\mathbf{u}} \cdot \delta(x - D) \tag{6}$$

subject to constraints such that $\mathbf{v_i}(\mathbf{x})$ is 0 with $x = 0$. This results in an implicit differential equation for filament segments which can be discretized and integrated in time to produce a solution for the motion of the system.

E. Computational Simulation Method

We tested our analytical conclusions on a computational model. More technical details of the model can be found in the Appendix, but we summarize the main modeling points here.

We discretize the filaments such that the equations of motion becomes a coupled system of equations for the velocities of filament endpoints, $\mathbf{x}$. The drag-like force between overlapping filaments results in a coupling of the velocities of endpoints.

$$\mathbf{A} \cdot \dot{\mathbf{x}} = \mathbf{f}(\mathbf{x}) \tag{7}$$

where $\mathbf{A}$ represents a coupling matrix between endpoints of filaments that overlap, and $\mathbf{f}(\mathbf{x})$ is the spring force between pairs of filament segment endpoints. We can then numerically integrate this system of equations to find the time evolution of the positions of all filament endpoints.

We generate a network by laying down filaments with random position and orientation within a domain of size $2D$ by D with periodic boundaries. The external stress (shear or extensional/compressional) is applied to all filament endpoints falling within a fixed x-distance from the center of the domain. Finally, filament endpoints falling within a fixed x-distance from the edges of the domain are constrained to be nonmoving.

The nominal units for length, force, and time are μm, nN, and s, respectively. We explored parameter space around an estimate of biologically relevant parameter values, given in Table

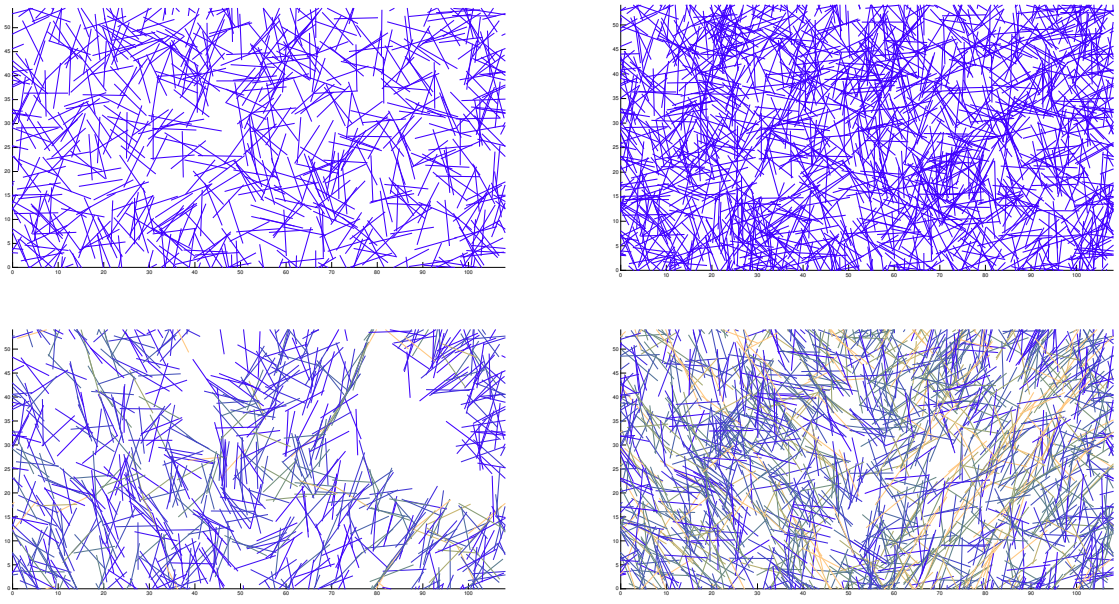

FIG. 1. Two Simulation setups with $L = 9\mu m, D = 54\mu m$ before (top) and after (bottom) 1000 seconds of applied stress. a) low density $l_c = 2\mu m$, b) moderate density $l_c = 1\mu m$

I.

TABLE I. Simulation Parameter Values

parameter	**symbol**	**estimated physiological value**	**smallest value**	**largest value**
extensional modulus	μ	$1nN$	$0.01nN$	$10nN$
bending modulus	κ	$10^{-3}nN \cdot \mu m$	-	-
cross-link drag coefficient	ξ	$?\frac{nNs}{\mu m}$	$1\frac{nNs}{\mu m}$	$10000\frac{nNs}{\mu m}$
medium drag coefficient	ζ	$0.0005\frac{nNs}{\mu m^2}$	$0.0005\frac{nNs}{\mu m^2}$	$0.01\frac{nNs}{\mu m^2}$
filament length	L	$5\mu m$	$1\mu m$	$10\mu m$
cross-link spacing	l_c	$0.5\mu m$	$0.1\mu m$	$2\mu m$
domain size	D	$10 - 50\mu m$	$4 \cdot L$	$10 \cdot L$

For computational simplicity in these models, unless otherwise mentioned we assume that the bending rigidity, κ, is infinite. This allows us to model filaments as non-bending springs of rest length, L, and spring modulus μ. In the appendix, we show that our result is not significantly different from the result for semi-flexible polymers.

III. RESULTS (WILL BE BROKEN UP)

A. Low Strain Approximation of Effective Viscosity

We begin with a calculation of a low-strain rate estimate of the effective viscosity for a network described by our model in the limit of highly rigid filaments. We carry this out by assuming we have applied a constant stress along a transect of the network. With moderate stresses, we assume the network reaches a steady state affine creep. In this situation, we would find that the stress in the network exactly balances the sum of the drag-like forces from cross-link slip. So for any transect of length D, we have a force balance equation.

$$\sigma = \frac{1}{D} \sum_{filaments} \sum_{crosslinks} \xi \cdot (\mathbf{v_i} - \mathbf{v_0}) \tag{8}$$

where $\mathbf{v_i}(\mathbf{s}) - \mathbf{v_j}(\mathbf{s})$ is the difference between the velocity of a filament at it's cross-link point and the velocity of the filament to which it is a attached. We can convert the sum over cross-links to an integral over the length using the average density of cross-links, $1/l_c$ and invoking the assumption of (linear order) affine strain rate, $\mathbf{v_i} - \mathbf{v_0} = \dot{\gamma} x$. This results in

$$\sigma = \frac{1}{D} \sum_{filaments} \xi \cdot \int_0^L ds \, (\mathbf{v}(\mathbf{s}) - \mathbf{v_0}(\mathbf{s})) \, \frac{1}{l_c}$$
$$= \sum_{filaments} \frac{\xi \dot{\gamma} L}{l_c} \cos\theta \cdot (x_l + \frac{L}{2} \cos\theta) \tag{9}$$

Here we have introduced the variables x_l, and θ to describe the leftmost endpoint and the angular orientation of a given filament respectively. Next, to perform the sum over all filaments we convert this to an integral over all orientations and endpoints that intersect our line of stress. We assume for simplicity that filament stretch and filament alignment are negligible in this low strain approximation. Therefore, the max distance for the leftmost endpoint is the length of a filament, L, and the maximum angle as a function of endpoint is $\arccos(x_l/L)$. The linear density of endpoints is the constant $D/l_c L$ so our integrals can be rewritten as this density over x_l and θ between our maximum and minimum allowed bounds.

$$\sigma = \frac{1}{D} \int_0^L dx_l \int_{-\arccos(\frac{x_l}{L})}^{\arccos(\frac{x_l}{L})} \frac{d\theta}{\pi} \frac{\xi \dot{\gamma} L}{l_c} \cdot \frac{D}{L l_c} \cdot (x_l \cos\theta + \frac{L}{2} cos^2\theta) \tag{10}$$

Carrying out the integrals and correcting for dangling filament ends leaves us with a relation between stress and strain rate.

$$\sigma = \frac{(L - 2l_c)^2 \xi}{4\pi l_c^2} \dot{\gamma} \tag{11}$$

We recognize the constant of proportionality between stress and strain rate as a viscosity. Therefore, our approximation for the effective viscosity, η_{eff}, at steady state creep in this low strain limit is

$$\eta_{eff} = \frac{(L - 2l_c)^2 \xi}{4\pi l_c^2}. \tag{12}$$

With moderate strains ($\gamma < 0.2$), our simulations show that in the high density limit, our theoretical approximation from Eqn 12 is highly accurate at explaining the network behavior. Aside from a geometrical factor, our approximation is valid for both shear and extensional stresses applied to the network.

As the density of the network approaches the breakdown limit, the effective viscosity diverges from our expected value. At the low connectivity limit, our expected viscosity goes to 0, but the medium viscosity begins to take over as we cross the percolation threshold.

In addition to changing the architecture and effective drag coefficient, we also validated the generality of our approximation by varying simulation size, medium viscosity, filament stiffness, and applied stress. We were able to find a slight trend that depended on filament stiffness as indicated in the difference between blue and red data points in Figure 2. This deviation from our approximation manifested itself more strongly when filaments were highly compliant, and we therefore interpret this as a higher order manifestation of the strain induced reordering of our networks which we focus on in the next section.

B. Effects from Large Strain

Large scale reorientation of cross-linked filaments under strain is a subject of active research at the moment [Sayantan]. Therefore, we wished to use our computational approach to extend our understanding of generic filament networks in the regime of shear induced anisotropy. Because we allowed variation in both the extensibility of individual filaments and the drag-like coupling between filaments, we found that we could induce reordering from high strain via either large filament compliance or large slip (or both).

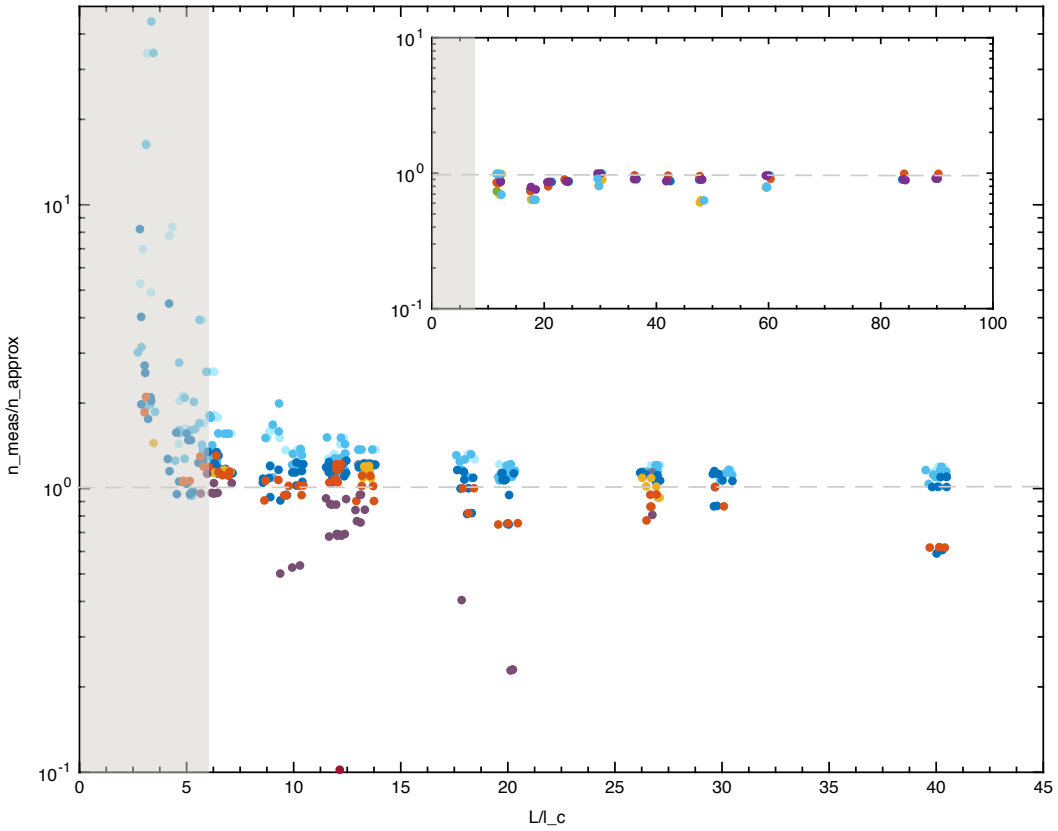

FIG. 2. Ratio of effective viscosity measured by shear simulation to predicted effective viscosity as a function of connectivity, L/l_c. Inset: Same measurement for extensional simulations

In Figure 3, we illustrate the four stereotyped phases of the general mechanical behavior that we observed in our networks. A deforming network typically undergoes a rapid filament stretching, a slower relaxation of elastic constraints, a phase of purely viscous cross-link slippage, and an eventual alignment and breakdown of network connectivity.

However, it isn't immediately clear how large these components of the strain will be or over what timescale they might take effect. If the filaments are highly rigid, there may be no significant stretching of filaments and the system may enter immediately into the cross-link slippage phase. If cross-link slippage is fast, the network may almost immediately align and tear apart.

To better understand to what extent and over what timescale each phase dominates the system behavior, we sought to determine the dependence of these effects on the microscopic

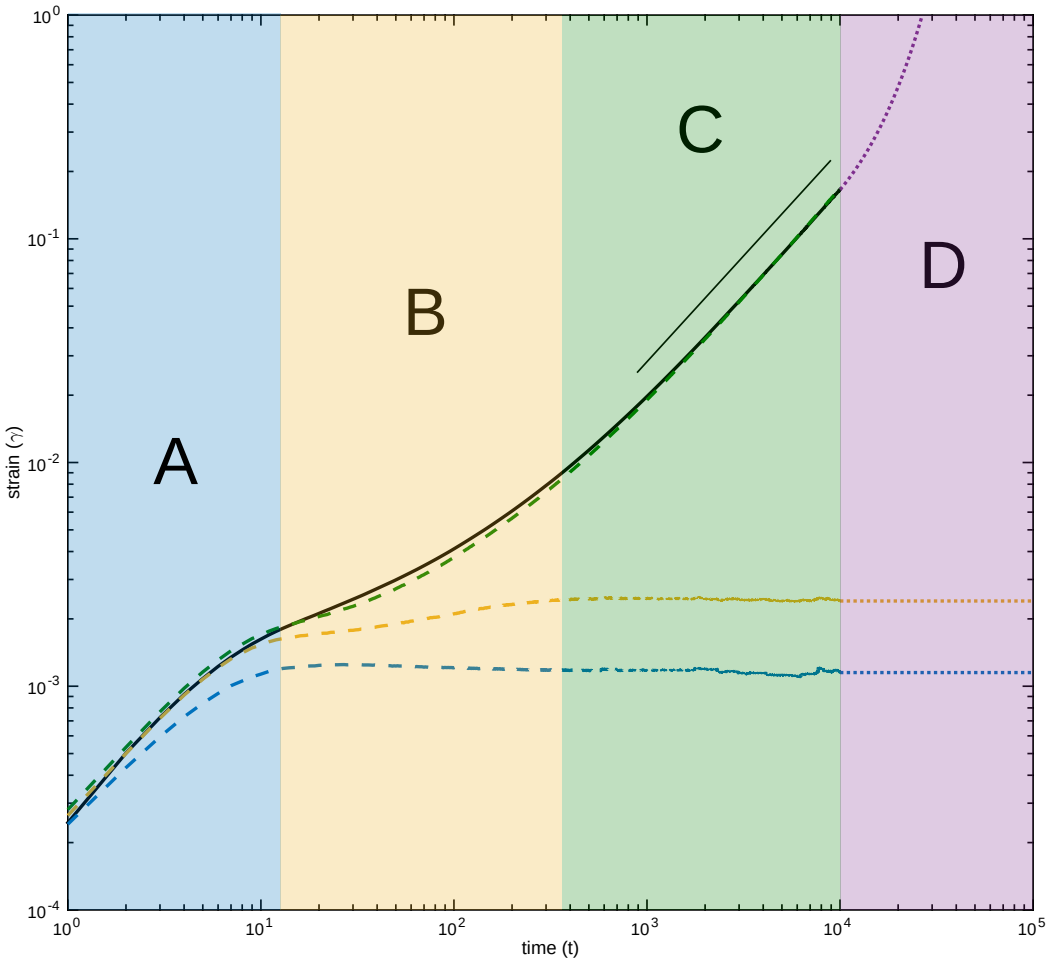

FIG. 3. Schematic of the general creep response of compliant filament networks illustrating the 4 phases of deformation: a) rapid mechanical response, b) combination of slow filament stretching and cross-link slip, c) cross-link slip dominated, d) network tearing from filament alignment. Note that the portion of the curve in section d is only a hypothetical continuation of the actual data.

parameters of our model. As the implications for each phase are quite different, we address each case separately.

1. *Phase B: Transient Softening from Slow Filament Stretch*

In general, filament stretch plays a part in two separate mechanical responses. In the first response, immediately after the application of an external stress, we see a rapid stretching

and compression of filaments (Phase A). This phase corresponds to the elastic relaxation of filament degrees of freedom allowed in the irreversibly cross linked case such as [17, 46].

Perhaps more interestingly, in the presence of cross-link slip, the interplay between filament stretching and cross-link slip gives rise to a second relaxation phase that deviates from both purely elastic and purely viscous behavior. During the first phase, filaments underwent large-scale dilation or contraction depending on their orientation relative to the direction of shear. However, some fraction of the filaments are still "under-stretched" due to local constraints from cross-links. These filaments are able to stretch farther as constraints from the cross-linking points slip, leading to an apparent viscous dissipation that decays away as filaments reach their stressed equilibrium length.

We see a broadening of the filament stretch distribution away from the affine approximation $\langle \delta L/L \rangle_0 = \gamma_{xy} sin(\theta) cos(\theta)$. Assuming that this broadening appears as a normally distributed variation in filament stretched length throughout the network ($\mathcal{N}$) with a time varying standard deviation, $\sigma(t)$, we have $\delta L/L = \langle \delta L/L \rangle_0 + \sigma(t) \cdot \mathcal{N}$.

This has an effect on the total mechanical energy stored in the network $\mathcal{H} \sim \langle \delta L/L \rangle^2 = \langle \delta L/L \rangle_0^2 + \sigma(t)^2$. Thus, the network will appear less viscous while some strain energy is being stored in the further stretching filaments.

In Figure 4, we illustrate using different compliance conditions that the slope of the creep curves only becomes constant after the spread in the filament length, σ, has reached a steady value. This implies that the long-lived sub-viscous creep behavior occurs during the period over which the distribution of filament extension is changing.

Eventually the contribution from slow filament stretching will become negligible compared to that from pure cross-link slip on rigid rods. This occurs on a timescale similar to that of cross-link slip and causes the effective viscosity to decay back toward the rigid limit. This gives rise to a less-than-linear creep response during times after the initial elastic relaxation but before full filament relaxation from cross-link slip. As shown in Figure 5, the transition begins to take place as network strain reaches 10 to 100 times the strain from pure mechanical stretching, $\delta L/L$, and this property is independent of the rate of strain.

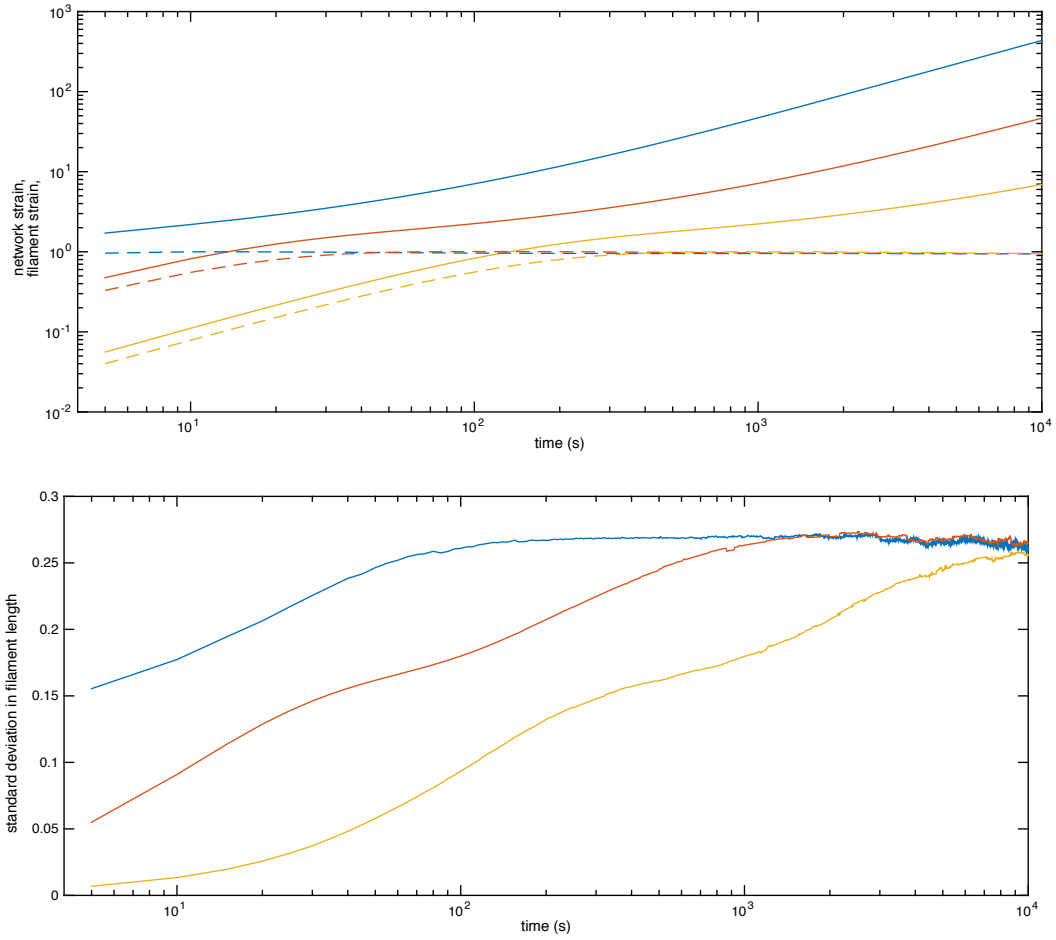

FIG. 4. Creep response of networks and filament extension for different filament compliances. A. Plot of total strain normalized by the strain from affine mechanical stretching, $\delta L/L$. Dashed lines show the amount of strain from affine mechanical stretching. B. Standard deviation of filament extension for the networks in A. Note that the creep compliance in A becomes constant (slope 1) only after the spread in filament extension in B stops increasing.

2. Phase D: Alignment at High Strain and Network Tearing

Once the network is able to accumulate a large strain, the assumption of nearly uniform distributions of filament orientations begins to break down.

At this point the filament orientations become unevenly distributed $\langle \delta L/L \rangle \neq \gamma_{xy} sin(\theta) cos(\theta)$, with a larger number of filaments aligning in the direction of extension rather than compression. Filament alignment, conceptually, causes the formation of subdomains that no longer span the space of the network. To the authors' knowledge an exact derivation of the

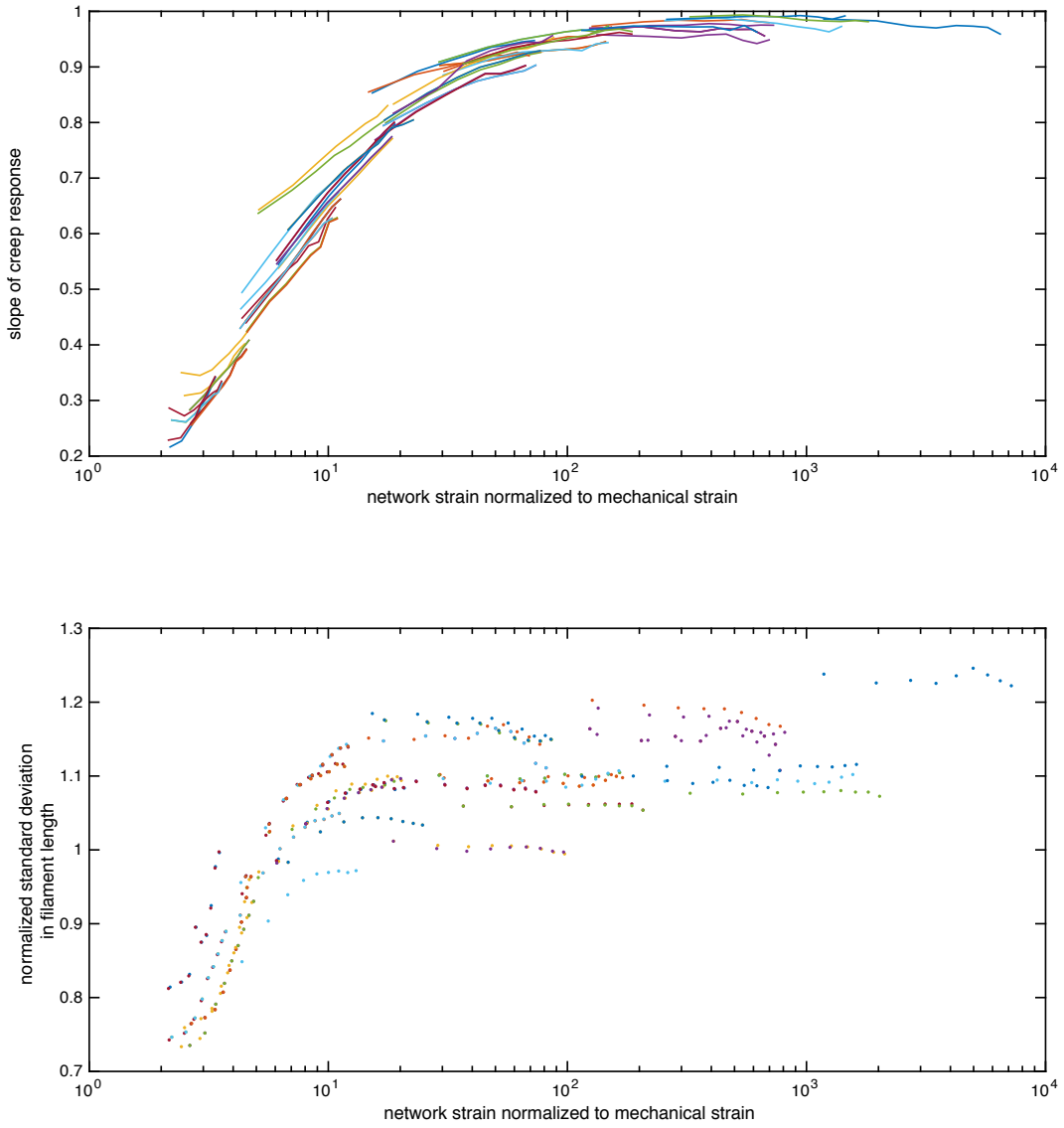

FIG. 5. A. Dependence of strain rate exponent as a function of strain relative to pure mechanical strain, $\delta L/L$. Individual colored lines represent individual strain simulations with varying simulation parameters. B. Corresponding standard deviation in filament strain, σ, as a function of strain relative to pure mechanical strain.

dependence of network connectedness on filament alignment has not been carried out, but Monte Carlo simulations have been used to show that alignment does indeed lead to lower connectedness[10].

Although a lengthy discussion of this behavior would be valuable, we've found the computational cost of exploring these kinds of alignment tearing networks to be prohibitive in their study at this time. Instead we now focus on just a few examples to garner some understanding.

We find that over time, the orientational distribution of the filaments begins to peak around 45 degrees as the large strain induces alignment. In Figure 6, we see that as the angular standard deviation falls, this reorientation eventually leads to be fewer bonds bridging the network perpendicular to the line of strain. As this connectivity begins to noticeably decrease, the observed effective viscosity decreases as well, giving rise to supralinear creep. From the inset of Figure 6 we can also see that the onset of phase D occurred before the network had completely reached phase C, leading to a rapid transition between sub-linear and super-linear creep response. Finally, it should be noted that the end of this simulation resulted in the network tearing apart.

C. Phase Diagram of Dominant Behavior

Finally, to explore the transitions between the various phases, we measured the creep response for a computationally tractable network ($L/l_c = 25$), as we varied the filament extensional modulus, μ, and the cross-link friction coefficient, ξ. In Figure 7 , we can see the trends for the transitions between phases A, B, and C. The line for the transition to D is still speculative at this time.

D. Frequency dependent modulus

This section will include a figure on the frequency dependent modulus once I get those.

IV. SUMMARY AND CONCLUSIONS

Conclusions I will draw after discussing the results with others.

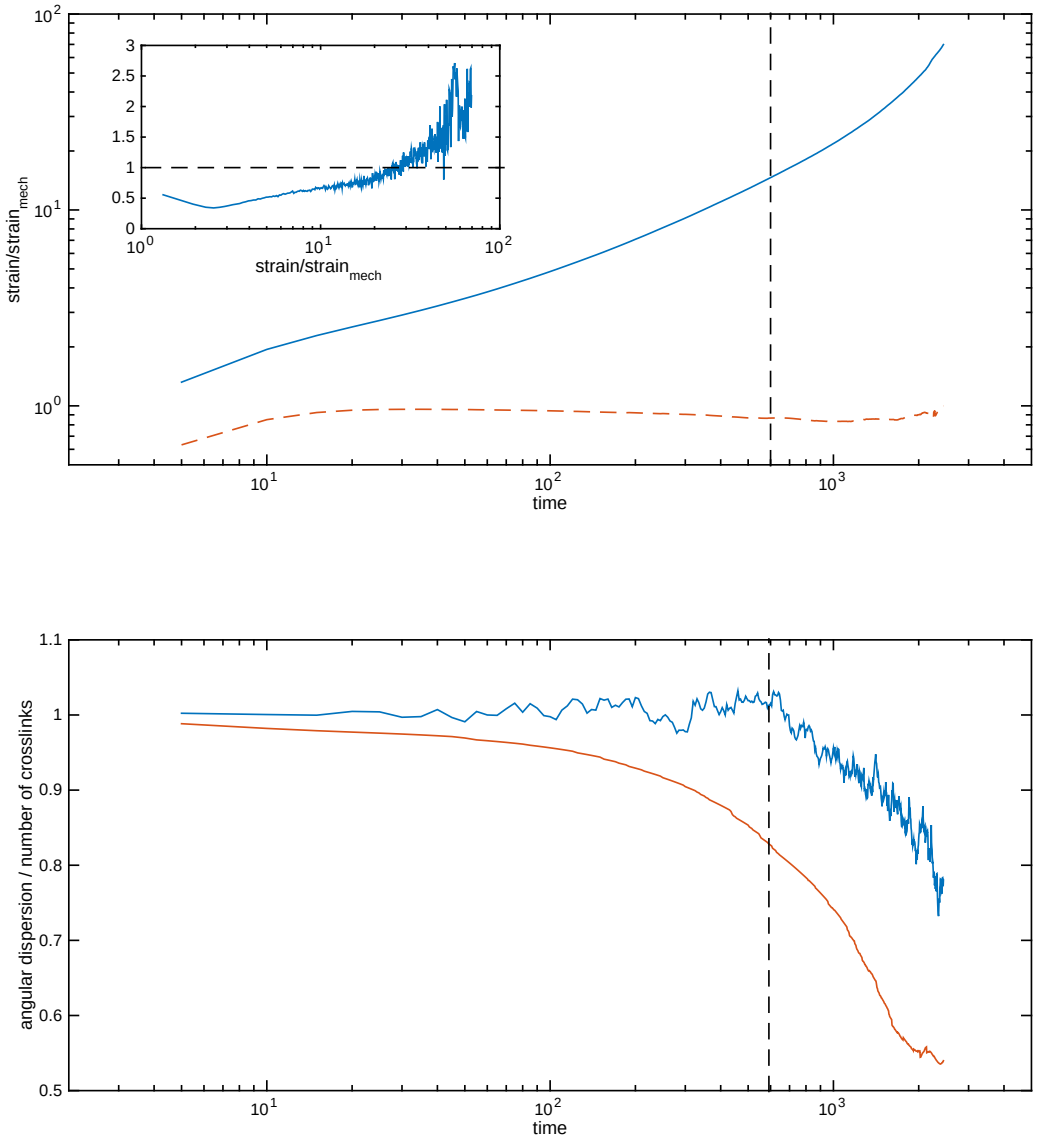

FIG. 6. A. Creep response of a network transitioning to phase D. Inset shows strain exponent as a function of strain (exponent passes 1). B. Traces for the relative angular dispersion and relative number of cross links corresponding to the same simulation as part A.

V. ACKNOWLEDGEMENTS

I'd like to thank Shiladitya Banerjee and Sayantan Majumdar for discussions on this topic. Hopefully I can thank other people after I've spoken with them.

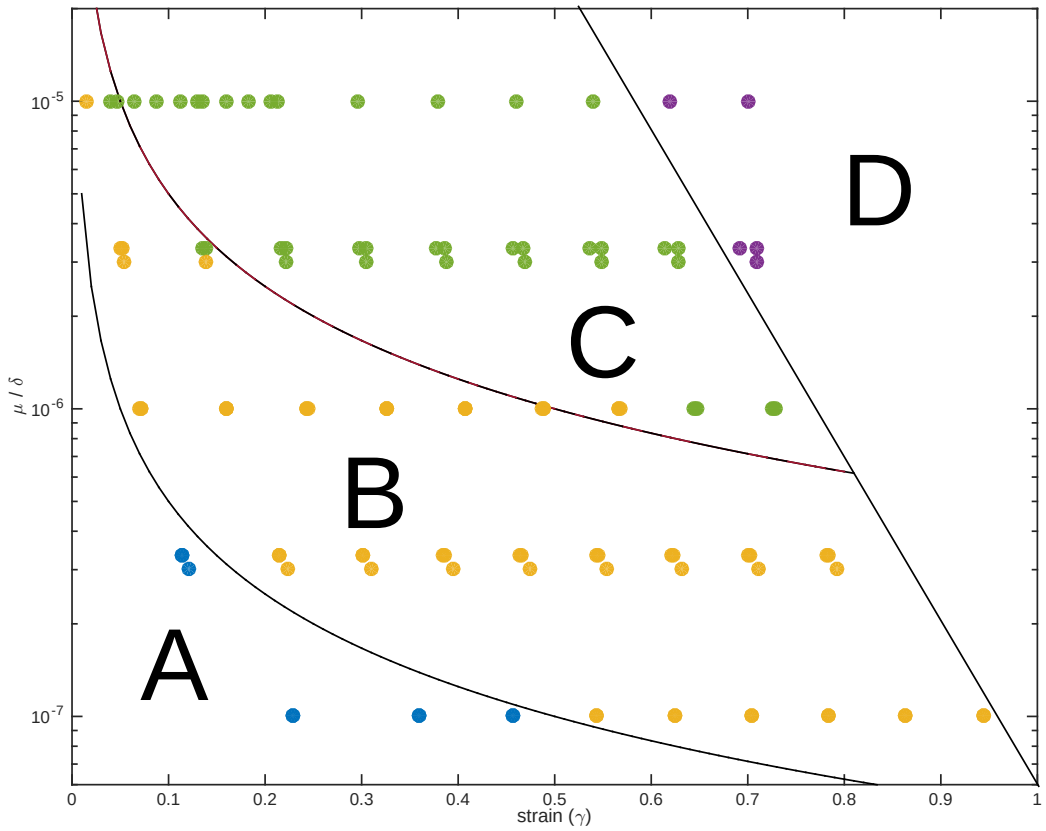

FIG. 7. phase diagram of creep response for different filament extension, μ and cross-link friction, δ. Yellow, green, and purple dots correspond to creep measurements $\gamma \sim t^{\alpha}$ with $\alpha < 0.92$, $0.92 < \alpha < 0.98$, or $\alpha > 0.98$ respectively. Blue dots represent creep measurements where $\gamma_{total} < 2\gamma_{mechanical}$

Appendix A: Network Tearing under Extensional Stress

1. Extensional Thinning and Network Tearing

For moderate extensional stresses, the rigid filament approximation of the effective viscosity simply picks up a different geometrical factor out front.

However, at higher stress and in the presence of different things happen.

$$\frac{\partial l_c}{dt} = l_c\dot{\gamma} = \frac{l_c\sigma}{\eta} \sim l_c^3\frac{\sigma}{L^2\xi} \tag{A1}$$

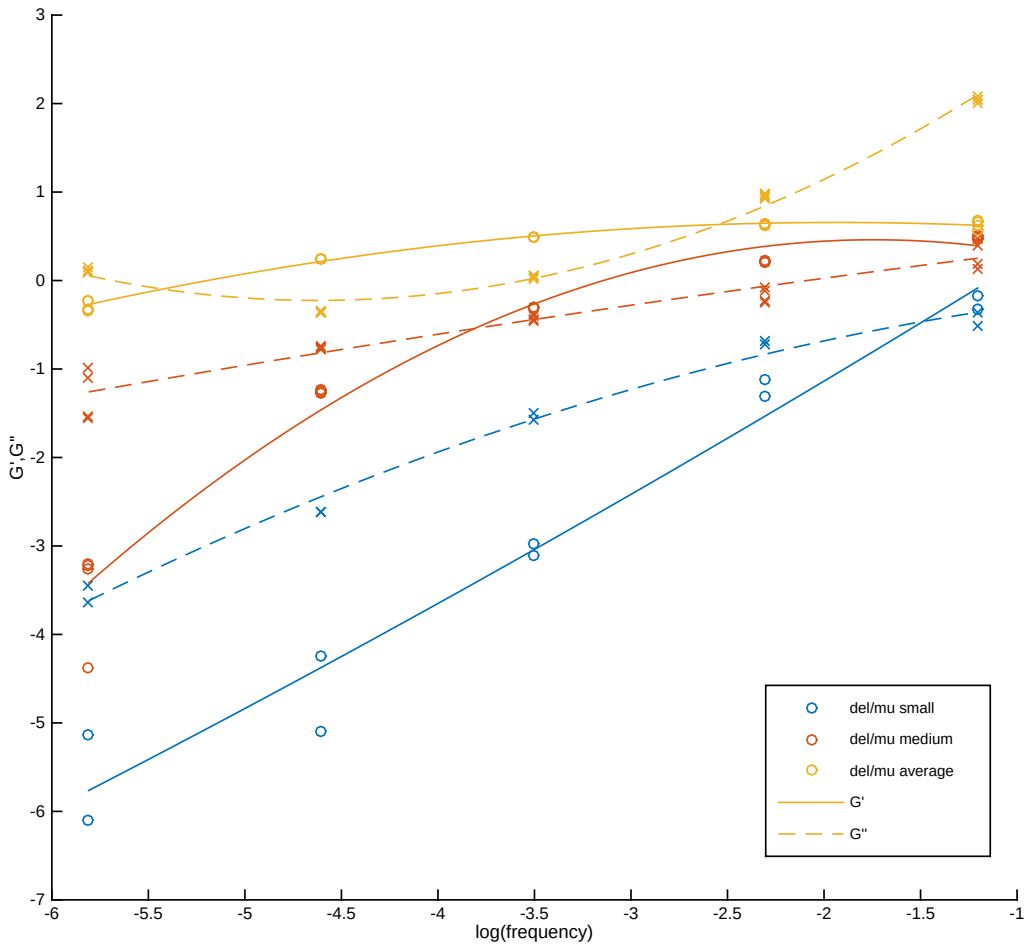

FIG. 8. Frequency dependent moduli for networks.

We can see that the rate of network thinning accelerates as we would expect. When the network reaches some minimum connectivity we assume that it stops behaving as a continuum material and the network tears irreversibly.

$$\tau_{break} = \frac{\eta_{eff}}{2\sigma} \cdot \left(1 - \frac{l_c^2}{l_{break}^2}\right) \tag{A2}$$

This provides us with an estimate of the timescale of catastrophic breakdown for a network with a given initial architecture and molecular drag.

2. Tearing Events During Extensional Strain

This behavior is caused primarily by the low density network undergoing tearing events that interrupt global connectedness.

Appendix B: Deriving Molecular Drag Coefficients

Thus far, the idea of a molecular drag coefficient was taken as a phenomenological, measured parameter for a given experimental setup. While this is a sufficient pragmatic justification, it's useful to try to motivate the quantitative value of this drag coefficient by connecting it to the underlying cross-link properties of binding affinity, concentration, and extensibility.

To do this we'll imagine the simplified case of two cross linkers sliding past each other in one dimension. In this case, assume that we have an equilibrium number of bound cross-linkers, n_B, each of which is displaced from its equilibrium length by some distance x. Each cross linker unbinds with rate k_{off} and rebinds at it's relaxed position ($x = 0$) with rate k_{on}. At the same time, all the cross linkers are being pulled from their relaxed position at a rate, v, which is simply the rate at which the filaments are sliding past each other.

We can right down an equation for the change in the density of cross-links at displacement x as they are pulled upon, bind, and unbind.

$$\frac{\partial \rho}{\partial t} = -k_{off}\rho(x) - v\frac{\partial \rho}{\partial x} + k_{on}\delta(x) \tag{B1}$$

Recognizing that $\int \rho(x) = n_B$ implies $k_{on} = k_{off}n_B$, we can find the steady state solution

$$\rho(x) = \frac{n_b k_{off}}{v} \cdot exp\left(-\frac{k_{off}}{v}x\right) \tag{B2}$$

If each cross-link has a spring constant μ_c, then we can equate the force on all cross-links to the applied force that is sliding the filaments past each other. Realistically, the spring constant and binding affinity would be functions of the cross-link stretch, but here we are taking them as approximately constant.

$$\int_0^\infty \rho(x)\mu_c x dx = v\frac{\mu_c n_B}{k_{off}} = F_{app} \tag{B3}$$

a

Therefore, the term next to v, (i.e. $\frac{\mu_c n_B}{k_{off}}$) would be equal to our molecular drag coefficient, ξ. assuming, approximately 1-5 cross links per filament overlap, and using the following table of estimates pulled from Ferrer et al., we can chart the accuracy of this simple predictive model.

cross-linker type	α-actinin	filamin-A
dissociation constant (s^{-1})	0.4	0.6
spring constant ($nN/\mu m$)	455	820
drag coefficient ($\frac{nN \cdot s}{\mu m}$)	200-1000	500-2500

This molecular description assumed both a constant off-rate and linear force extension of cross-links. In the event that binding kinetics are regulated by the state of extension, we would expect (based on Rf) to find a region that exhibits a stick-slip behavior instead of the smooth. Depending on the nature of any coupling between cross-links local stick-slip could either give rise to a global stick-slip behavior or a heterogenous mixture of stuck and sliding cross-links. It would be interesting to explore this topic further in the future, but in the present analysis, we choose to ignore complications from these nonlinear effects.

Appendix C: Deriving Filament and Cross-Link Composite Extensional Modulus

Section describing how you derive the extensional modulus.

---

[1] Shiladitya Banerjee, M. Cristina Marchetti, and Kristian Müller-Nedebock. Motor-driven dynamics of cytoskeletal filaments in motility assays. *Phys. Rev. E*, 84:011914, Jul 2011.

[2] Andreas R. Bausch, Florian Ziemann, Alexei A. Boulbitch, Ken Jacobson, and Erich Sackmann. Local measurements of viscoelastic parameters of adherent cell surfaces by magnetic bead microrheometry. *Biophysical Journal*, 75(4):2038 – 2049, 1998.

[3] D Bray and JG White. Cortical flow in animal cells. *Science*, 239(4842):883–888, 1988.

[4] C. P. Broedersz, C. Storm, and F. C. MacKintosh. Effective-medium approach for stiff polymer networks with flexible cross-links. *Phys. Rev. E*, 79:061914, Jun 2009.

[5] Chase P. Broedersz, Martin Depken, Norman Y. Yao, Martin R. Pollak, David A. Weitz, and Frederick C. MacKintosh. Cross-link-governed dynamics of biopolymer networks. *Phys. Rev. Lett.*, 105:238101, Nov 2010.

[6] P. Broedersz, C. and C. MacKintosh, F.˙Modeling semiflexible polymer networks. *Rev. Mod. Phys.*, 86:995–1036, Jul 2014.

[7] Preethi L. Chandran and Mohammad R. K. Mofrad. Averaged implicit hydrodynamic model of semiflexible filaments. *Phys. Rev. E*, 81:031920, Mar 2010.

[8] Christian J. Cyron, Kei W. Müller, Andreas R. Bausch, and Wolfgang A. Wall. Micromechanical simulations of biopolymer networks with finite elements. *Journal of Computational Physics*, 244(0):236 – 251, 2013. Multi-scale Modeling and Simulation of Biological Systems.

[9] M. Doi and S. F. Edwards. *The Theory of Polymer Dynamics*. Oxford University Press, USA, November 1986.

[10] Fangming Du, John E. Fischer, and Karen I. Winey. Effect of nanotube alignment on percolation conductivity in carbon nanotube/polymer composites. *Phys. Rev. B*, 72:121404, Sep 2005.

[11] E Evans and A Yeung. Apparent viscosity and cortical tension of blood granulocytes determined by micropipet aspiration. *Biophysical Journal*, 56(1):151–160, 07 1989.

[12] A. E. Filippov, J. Klafter, and M. Urbakh. Friction through dynamical formation and rupture of molecular bonds. *Phys. Rev. Lett.*, 92:135503, Mar 2004.

[13] Daniel A. Fletcher and R. Dyche Mullins. Cell mechanics and the cytoskeleton. *Nature*, 463(7280):485–492, 01 2010.

[14] M. L. Gardel, F. Nakamura, J. Hartwig, J. C. Crocker, T. P. Stossel, and D. A. Weitz. Stress-dependent elasticity of composite actin networks as a model for cell behavior. *Phys. Rev. Lett.*, 96:088102, Mar 2006.

[15] M. L. Gardel, F. Nakamura, J. H. Hartwig, J. C. Crocker, T. P. Stossel, and D. A. Weitz. Prestressed f-actin networks cross-linked by hinged filamins replicate mechanical properties of cells. *Proceedings of the National Academy of Sciences of the United States of America*, 103(6):1762–1767, 2006.

[16] M. L. Gardel, J. H. Shin, F. C. MacKintosh, L. Mahadevan, P. Matsudaira, and D. A. Weitz. Elastic behavior of cross-linked and bundled actin networks. *Science*, 304(5675):1301–1305, 2004.

[17] David A. Head, Alex J. Levine, and F. C. MacKintosh. Deformation of cross-linked semiflexible polymer networks. *Phys. Rev. Lett.*, 91:108102, Sep 2003.

[18] Claus Heussinger, Boris Schaefer, and Erwin Frey. Nonaffine rubber elasticity for stiff polymer networks. *Phys. Rev. E*, 76:031906, Sep 2007.

[19] S N Hird and J G White. Cortical and cytoplasmic flow polarity in early embryonic cells of caenorhabditis elegans. *The Journal of Cell Biology*, 121(6):1343–1355, 1993.

[20] Robert M Hochmuth. Micropipette aspiration of living cells. *Journal of Biomechanics*, 33(1):15 – 22, 2000.

[21] Paul A. Janmey, Soren Hvidt, Jennifer Lamb, and Thomas P. Stossel. Resemblance of actin-binding protein/actin gels to covalently crosslinked networks. *Nature*, 345(6270):89–92, 05 1990.

[22] K. E. Kasza, C. P. Broedersz, G. H. Koenderink, Y. C. Lin, W. Messner, E. A. Millman, F. Nakamura, T. P. Stossel, F. C. MacKintosh, and D. A. Weitz. Actin filament length tunes elasticity of flexibly cross-linked actin networks. *Biophysical Journal*, 99(4):1091–1100, 2015/03/12.

[23] Taeyoon Kim, Wonmuk Hwang, and Roger D Kamm. Dynamic role of cross-linking proteins in actin rheology. *Biophysical Journal*, 101(7):1597–1603, 10 2011.

[24] Gijsje H Koenderink, Zvonimir Dogic, Fumihiko Nakamura, Poul M Bendix, Frederick C MacKintosh, John H Hartwig, Thomas P Stossel, and David A Weitz. An active biopolymer network controlled by molecular motors. *Proceedings of the National Academy of Sciences of the United States of America*, 106(36):15192–15197, 09 2009.

[25] O. Lieleg and A. R. Bausch. Cross-linker unbinding and self-similarity in bundled cytoskeletal networks. *Phys. Rev. Lett.*, 99:158105, Oct 2007.

[26] O. Lieleg, M. M. A. E. Claessens, Y. Luan, and A. R. Bausch. Transient binding and dissipation in cross-linked actin networks. *Phys. Rev. Lett.*, 101:108101, Sep 2008.

[27] O. Lieleg, K. M. Schmoller, M. M. A. E. Claessens, and A. R. Bausch. Cytoskeletal polymer networks: Viscoelastic properties are determined by the microscopic interaction potential of cross-links. *Biophysical Journal*, 96(11):4725–4732, 6 2009.

[28] Oliver Lieleg, Mireille M. A. E. Claessens, and Andreas R. Bausch. Structure and dynamics of cross-linked actin networks. *Soft Matter*, 6:218–225, 2010.

[29] Yi-Chia Lin, Chase P. Broedersz, Amy C. Rowat, Tatjana Wedig, Harald Herrmann, Frederick C. MacKintosh, and David A. Weitz. Divalent cations crosslink vimentin intermediate filament tail domains to regulate network mechanics. *Journal of Molecular Biology*, 399(4):637 – 644, 2010.

[30] J. Liu, G. H. Koenderink, K. E. Kasza, F. C. MacKintosh, and D. A. Weitz. Visualizing the strain field in semiflexible polymer networks: Strain fluctuations and nonlinear rheology of f-actin gels. *Phys. Rev. Lett.*, 98:198304, May 2007.

[31] John F. Marko and Eric D. Siggia. Stretching dna. *Macromolecules*, 28(26):8759–8770, 1995.

[32] Mirjam Mayer, Martin Depken, Justin S. Bois, Frank Julicher, and Stephan W. Grill. Anisotropies in cortical tension reveal the physical basis of polarizing cortical flows. *Nature*, 467(7315):617–621, 09 2010.

[33] David C. Morse. Viscoelasticity of concentrated isotropic solutions of semiflexible polymers. 2. linear response. *Macromolecules*, 31(20):7044–7067, 1998.

[34] Kei W. Müller, Robijn F. Bruinsma, Oliver Lieleg, Andreas R. Bausch, Wolfgang A. Wall, and Alex J. Levine. Rheology of semiflexible bundle networks with transient linkers. *Phys. Rev. Lett.*, 112:238102, Jun 2014.

[35] Michael P. Murrell and Margaret L. Gardel. F-actin buckling coordinates contractility and severing in a biomimetic actomyosin cortex. *Proceedings of the National Academy of Sciences*, 109(51):20820–20825, 2012.

[36] Guillaume Salbreux, Guillaume Charras, and Ewa Paluch. Actin cortex mechanics and cellular morphogenesis. *Trends in Cell Biology*, 22(10):536 – 545, 2012.

[37] Tim Sanchez, Daniel T. N. Chen, Stephen J. DeCamp, Michael Heymann, and Zvonimir Dogic. Spontaneous motion in hierarchically assembled active matter. *Nature*, 491(7424):431–434, 11 2012.

[38] Evan Spruijt, Joris Sprakel, Marc Lemmers, Martien A. Cohen Stuart, and Jasper van der Gucht. Relaxation dynamics at different time scales in electrostatic complexes: Time-salt superposition. *Phys. Rev. Lett.*, 105:208301, Nov 2010.

[39] Dimitrije Stamenovic. Cell mechanics: Two regimes, maybe three? *Nat Mater*, 5(8):597–598, 08 2006.

[40] Cornelis Storm, Jennifer J. Pastore, F. C. MacKintosh, T. C. Lubensky, and Paul A. Janmey. Nonlinear elasticity in biological gels. *Nature*, 435(7039):191–194, 05 2005.

[41] R. Tharmann, M. M. A. E. Claessens, and A. R. Bausch. Viscoelasticity of isotropically cross-linked actin networks. *Phys. Rev. Lett.*, 98:088103, Feb 2007.

[42] Andrea Vanossi, Nicola Manini, Michael Urbakh, Stefano Zapperi, and Erio Tosatti. *Colloquium* : Modeling friction: From nanoscale to mesoscale. *Rev. Mod. Phys.*, 85:529–552, Apr 2013.

[43] D.H. Wachsstock, W.H. Schwarz, and T.D. Pollard. Cross-linker dynamics determine the mechanical properties of actin gels. *Biophysical Journal*, 66(3, Part 1):801 – 809, 1994.

[44] Andrew Ward, Feodor Hilitski, Walter Schwenger, David Welch, A. W. C. Lau, Vincenzo Vitelli, L. Mahadevan, and Zvonimir Dogic. Solid friction between soft filaments. *Nat Mater*, advance online publication:–, 03 2015.

[45] Sabine M. Volkmer Ward, Astrid Weins, Martin R. Pollak, and David A. Weitz. Dynamic viscoelasticity of actin cross-linked with wild-type and disease-causing mutant -actinin-4. *Biophysical Journal*, 95(10):4915 – 4923, 2008.

[46] Jan Wilhelm and Erwin Frey. Elasticity of stiff polymer networks. *Phys. Rev. Lett.*, 91:108103, Sep 2003.

[47] M. Wyart, H. Liang, A. Kabla, and L. Mahadevan. Elasticity of floppy and stiff random networks. *Phys. Rev. Lett.*, 101:215501, Nov 2008.

[48] Norman Y. Yao, Daniel J. Becker, Chase P. Broedersz, Martin Depken, Frederick C. MacKintosh, Martin R. Pollak, and David A. Weitz. Nonlinear viscoelasticity of actin transiently cross-linked with mutant -actinin-4. *Journal of Molecular Biology*, 411(5):1062 – 1071, 2011.